İSTANBUL UNIVERSITY PRESS

Physics and Astronomy Reports
PAR 2025, 3 (1), 1–12
DOI: 10.26650/PAR.2025.00003

RESEARCH ARTICLE

Comprehensive Analysis of Middle-Aged Open Cluster NGC 6793 in Vulpecula via Gaia DR3 Data

S. Taşdemir[1*], D. C. Çınar[1], R. Canbay[2], S. Taştan[2], W. H. Elsanhoury[3], and Haroon, A. A.[4,5]

[1]İstanbul University, Institute of Graduate Studies in Science, Programme of Astronomy and Space Sciences, 34116, Beyazıt, İstanbul, Türkiye
[2]İstanbul University, Faculty of Science, Department of Astronomy and Space Sciences, 34119, Beyazıt, İstanbul, Türkiye
[3]Northern Border University, Department of Physics, College of Science, Arar, Saudi Arabia
[4]King Abdulaziz University,Faculty of Science, Department of Astronomy and Space Science, Jeddah, Saudi Arabia
[5]National Research Institute of Astronomy and Geophysics (NRIAG), Department of Astronomy, 11421, Helwan, Cairo, Egypt

ABSTRACT

We conducted an in-depth analysis of NGC 6793 open cluster via *Gaia* DR3 data, including astrometric, spectroscopic, and photometric measurements. A selection of 147 stars, which show membership probabilities $P \geq 0.5$ were classified as likely members. The mean trigonometric parallaxes and proper-motion components of the cluster were found to be $\varpi = 1.674 \pm 0.045$ mas and $(\mu_\alpha \cos\delta, \mu_\delta)$ =(3.814 ± 0.031, 3.547 ± 0.034) mas yr^{-1}. The fundamental astrophysical parameters of NGC 6793 are derived simultaneously as $t = 650 \pm 50$ Myr, $\mu = 9.508 \pm 0.070$ mag and $E(G_{BP} - G_{RP}) = 0.361 \pm 0.035$ mag. The cluster's luminosity function shows the G-absolute magnitude limit of its main stars, indicating a clear stellar population. The cluster's total mass, from the mass function with $P \geq 0.5$ stars, is estimated as $139 \pm 12\ M/M_\odot$. The slope of the MF was found to be $\Gamma = 1.40 \pm 0.26$, a result consistent with the Salpeter value. The kinematic analyses present velocity ellipsoid parameters as well as the convergent point $(A_o,\ D_o) = (85^\circ.85 \pm 0^\circ.11,\ 3^\circ.12 \pm 0^\circ.57)$. Analyses show that it is moving in a box-shaped orbit beyond the Sun's galactic radius and belongs to the thin disk population of the Milky Way. The calculated relaxation time suggests that NGC 6793 has reached a dynamically relaxed state with the dynamical evolution parameter τ significantly exceeds one. These results show the cluster's stability and link to the thin disc population.

Keywords: Galaxy: open clusters and associations; individual: NGC 6793, Galaxy: Stellar kinematics, orbital and velocity ellipsoid parameters, stars: Hertzsprung Russell (HR) diagram.

1. INTRODUCTION

Open clusters (OCs) are stellar assemblies characterised by their gravitationally bound nature, comprising stars that have formed together within the same molecular cloud. This process, resulting in the collapse and disintegration of giant molecular clouds, is a fundamental aspect of star formation in the Milky Way (Lada & Lada 2003; Kroupa 2001). Consequently, the member stars of an OC share a common origin, which implies similarities in their chemical compositions (e.g., metallicity), distances from the Sun, and formation timescales. These shared properties make OCs prime targets for studies involving stellar populations and Galactic structure.

However, the masses of stars in open clusters vary considerably due to the complexity of star-forming processes. This mass variation is directly reflected in their broad range of luminosities, effective temperatures, and spectral types (Bastian et al. 2010). Furthermore, as clusters evolve, dynamical interactions such as mass segregation and tidal stripping can modify their internal structure and membership, providing valuable insights into both stellar and dynamical evolution (Binney & Tremaine 2008).

In addition to their utility in tracing the Galaxy's formation history, OCs serve as benchmarks for calibrating stellar evolutionary models. Their relatively young ages, often less than a few hundred million years, enable astronomers to study the early phases of stellar evolution, while older clusters, like M67, offer constraints on the later phases of stellar lifecycles (Perryman et al. 1998). These characteristics underscore the role of OCs as essential laboratories for investigating a wide array of astrophysical phenomena, from initial mass functions to the chemical evolution of the Galactic interstellar medium.

Previous studies have provided the following information regarding NGC 6793: NGC 6793 ($\alpha = 19^h23^m16^s.08, \delta = +22^\circ09'32''3$; $l = 56^\circ.1860, b = +03^\circ.3180$, J2000) is located in the Vulpecula constellation. Cantat-Gaudin et al. (2020) determined the astrophysical and astrometric parameters of more than 2,000 open clusters using the *Gaia* DR2 catalogue. In their analysis of NGC 6793, they identified 185 probable

Corresponding Author: S. Taşdemir **E-mail:** tasdemir.seval@ogr.iu.edu.tr
Submitted: 20.01.2025 • **Revision Requested:** 06.02.0025 • **Last Revision Received:** 08.03.2025 • **Accepted:** 21.03.2025 • **Published Online:** 16.06.2025

Table 1. The astrophysical parameters of NGC 6793, as gathered from available literature, include key measurements: colour excess ($E(B-V)$), heliocentric distance (d), metallicity ([Fe/H]), age (t), mean proper-motion components ($\langle\mu_\alpha\cos\delta\rangle$, $\langle\mu_\delta\rangle$), and mean radial velocity ($\langle V_R\rangle$).

$E(B-V)$ (mag)	d (pc)	[Fe/H] (dex)	t (Myr)	$\langle\mu_\alpha\cos\delta\rangle$ (mas yr^{-1})	$\langle\mu_\delta\rangle$ (mas yr^{-1})	$\langle V_R\rangle$ (km s^{-1})	Ref
0.331±0.119	586±0.53	—	309	3.799±0.011	3.535±0.012	-20.02±0.76	(01)
0.238	628	—	309	—	—	—	(02)
—	618	—	309	3.789±0.080	3.544±0.090	—	(03)
—	618	—	309	—	—	-37 ± 5.35	(04)
—	618	—	309	3.794±0.170	3.543±0.146	—	(05)
0.326±0.023	589±7	0.234±0.076	458±69	3.778±0.194	3.569±0.237	-25.68±4.71	(06)
0.238	—	—	650	3.795±0.186	3.544±0.177	—	(07)
0.330±0.004	610±40	-0.09±0.10	500±50	3.818±0.055	3.611±0.071	—	(08)
0.218±0.006	—	0.00	572±88	—	—	—	(09)
—	—	0.25	66±4	3.774±0.232	3.577±0.257	—	(10)
—	—	—	—	—	—	-16.59±1.45	(11)
0.312	724	—	495	—	—	—	(12)
0.256±0.025	585±19	0.10±0.05	650±50	3.814±0.031	3.547±0.034	-20.87±0.67	(13)

(01) Hunt & Reffert (2024), (02) Donada et al. (2023), (03) Tarricq et al. (2022), (04) Tarricq et al. (2021), (05) Poggio et al. (2021), (06) Dias et al. (2021), (07) Cantat-Gaudin et al. (2020), (08) Yontan et al. (2019) (09) Bossini et al. (2019), (10) Liu & Pang (2019), (11) Soubiran et al. (2018), (12) Joshi et al. (2016), (13) This study

members based on astrometric and photometric selection criteria. Using these members, they estimated the V-band extinction, distance modulus, distance, and age of the cluster as $A_V = 0.74$ mag, $(m-M) = 8.99$ mag, 628 pc, and 309 Myr, respectively. The proper-motion components were reported as $(\mu_\alpha\cos\delta, \mu_\delta) = (3.79 \pm 0.18, 3.54 \pm 0.18)$ mas yr^{-1}. Cantat-Gaudin et al. (2020) determined the astrophysical and astrometric parameters of more than 2,000 open clusters using the *Gaia* DR2 catalogue. In their analysis of NGC 6793, they identified 185 probable members based on astrometric and photometric selection criteria. Using these members, they estimated the V-band extinction, distance modulus, distance, and age of the cluster as $A_V = 0.74$ mag, $(m-M) = 8.99$ mag, 628 pc, and 309 Myr, respectively. The proper-motion components were reported as $(\mu_\alpha\cos\delta, \mu_\delta) = (3.79 \pm 0.18, 3.54 \pm 0.18)$ mas yr^{-1}.

CCD UBV analyses of the NGC 6793 via *Gaia* DR2 astrometric data were performed by Yontan et al. (2019). From 87 member stars, they determined reddening, distance, metallicity as $E(B-V)$= 0.33±0.04 mag, d=610±40 pc, [Fe/H]=-0.09±0.10 dex, respectively. Yontan et al. (2019) also derived the cluster age as 500±50 Myr.

Soubiran et al. (2018) conducted kinematic investigations of more than 800 OCs through *Gaia* DR2 database. For NGC 6793, based on 13 stars, they estimated the radial velocity $V_R = 24.32 \pm 0.73$ km s^{-1} and the mean space-velocity components as (U, V, W) = (-20.45 ± 0.81, -5.91 ± 1.20, -5.66 ± 0.09) km s^{-1}. Using Bayesian statistical techniques and *Gaia* DR2 data, Bossini et al. (2019) calculated the age of NGC 6793 to be $t = 572^{+90}_{-160}$ Myr. This determination helps explain the cluster's evolutionary stage and its position within the broader context of OCs. Table 1 shows the literature results of NGC 6793 to make comparison easier.

The structure of the paper is as follows: Section 2 provides a detailed overview of the both astrometric and photometric datasets used for NGC 6793. Section 3 describes the methodologies used to derive the structural parameters of stars within the open cluster, and focuses on the analysis of photometric membership probabilities and astrophysical parameters. Section 4 presents the distribution of member stars in well-defined both luminosity and mass functions. Evolving times of NGC 6793 are computed in Section 5 and their convergent point was drawn here in Section 6. Section 7 is devoted to Galactic orbital parameters. Finally, Section 8 offers a summary of the findings and conclusions.

2. DATA

2.1. Astrometric and Photometric Data

With the help of the precise photometric (G, G_{BP} and G_{RP}), astrometric ($\mu_\alpha\cos\delta, \mu_\delta$ and ϖ) and spectroscopic (V_R) data from the latest data release of *Gaia* (*Gaia* DR3, Gaia Collaboration et al. 2023), we constructed an extensive catalogue for NGC 6793. The equatorial coordinates were taken from the catalogue of Cantat-Gaudin & Anders (2020) are $\langle\alpha, \delta\rangle = (19^h23^m16^s.08, \delta = +22°09'32''.3)$, and we all stars within a 30 arcmin region centred onthe cluster were considered. The resulting catalogue includes 256,620 stars with G-apparent magnitudes $7 < G\ (\text{mag}) \leq 22$ interval. The star chart of the region around NGC 6793, obtained using the `POSS2UKSTU_RED` filter[1], is shown in Figure 1.

2.2. Photometric Completeness Limit

To derive accurate astrophysical and structural parameters for NGC 6793, the cluster's completeness limit must first be established. This is crucial for accurate parameter estimation. In the case of NGC 6793, the photometric completeness limit was determined by analysing the star counts according to various G magnitudes. As shown in Figure 2, the histogram reveals that the star count increases with brighter magnitudes up to a limit of $G = 20.50$ mag, after which it decreases, indicating the completeness limit. Therefore, in subsequent analyses, stars fainter than this threshold were excluded statistically.

For error estimation, the uncertainties in the *Gaia* DR3 data

[1] https://archive.stsci.edu/cgi-bin/dss_form

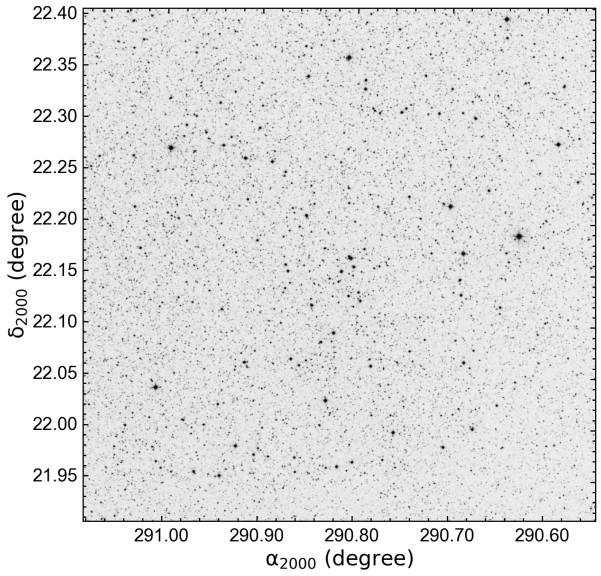

Figure 1. The star chart of NGC 6793. The field of view is $30' \times 30'$.

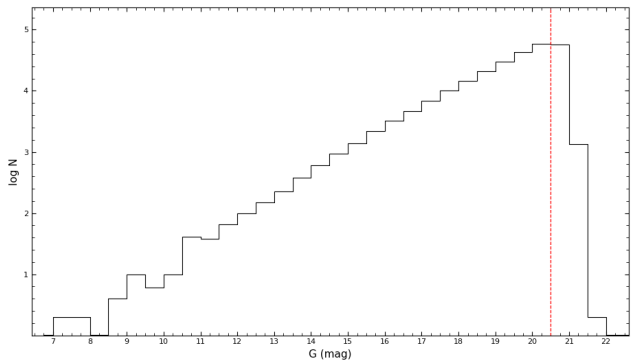

Figure 2. G-apparent magnitude histogram of stars in the direction of the NGC 6793 OC. The dashed line represents the faint-limiting magnitude.

were treated as interval errors. The mean G apparent magnitudes and $G_{BP} - G_{RP}$ colour indices of the stars in the open cluster field were calculated within G magnitude intervals. At the completeness limit of $G = 20.50$ mag, the mean internal G-apparent magnitude and $G_{BP} - G_{RP}$ colour index were found to be 0.007 and 0.142 mag, respectively. The mean photometric errors of NGC 6793 as a function of apparent G magnitudes are detailed in Table 2.

3. METHOD AND RESULTS

3.1. Structural Parameters of NGC 6793

To analyse the size and structure of NGC 6793, we performed a radial density profile (RDP) study. Using high-quality *Gaia* DR3 data within a 30 arcminute radius, the cluster region was divided into several concentric rings based on the central coordinates from Cantat-Gaudin et al. (2020). The stellar density, $\rho(r)$, was determined by selecting stars to the limiting apparent $G = 20.5$ mag. For each ring, the stellar density was calculated using the formula $R_i = N_i/A_i$, where N_i represents the number of stars in the i^{th} ring, and A_i is the corresponding area of that ring. To assess the uncertainties, we applied the Poisson statistical error formula $1/\sqrt{N}$, where N is the number of stars in the ring. Finally, the radial density profile was plotted, and

Table 2. Errors in the apparent magnitudes (G) and colours ($G_{BP} - G_{RP}$) of stars in the cluster direction.

G (mag)	N	σ_G (mag)	$\sigma_{G_{BP}-G_{RP}}$ (mag)
(7, 14]	816	0.003	0.008
(14, 15]	1,258	0.003	0.007
(15, 16]	2,911	0.003	0.007
(16, 17]	6,521	0.003	0.009
(17, 18]	13,904	0.003	0.016
(18, 19]	28,137	0.003	0.034
(19, 20]	55,495	0.005	0.078
(20, 21]	95,811	0.010	0.200
(21, 22]	16,193	0.028	0.426

the empirical model from King (1962) was used to fit the data:

$$\rho(r) = f_{bg} + \frac{f_o}{1 + (r/r_c)^2} \quad (1)$$

In this context, the radius of the cluster is represented by r. The parameters f_{bg}, f_o, and r_c refer to the stellar density of the background, the central stellar density, and the core radius, respectively. To derive the best estimates for these parameters, the χ^2 minimization technique was employed during the RDP fitting process. The solid black line in Figure 3 demonstrates the best-fit solution to the radial density profile. The goodness of fit, indicated by the correlation coefficient $R^2 = 0.967$, suggests a high degree of accuracy in the estimation of the structural parameters, supporting the reliability of the model.

Based on the analysis of the radial density profile (RDP), we calculated the limiting radius of the cluster, r_{lim}^{obs}, to be 10 arcmin. The derived structural parameters include $f_{bg} = 62.855 \pm 0.7502$, $f_0 = 89.628 \pm 5.878$ stars arcmin^{-2}, and $r_c = 1.593 \pm 0.128$ arcmin. To assess the reliability of the observed limiting radius (r_{lim}), we applied the formula from

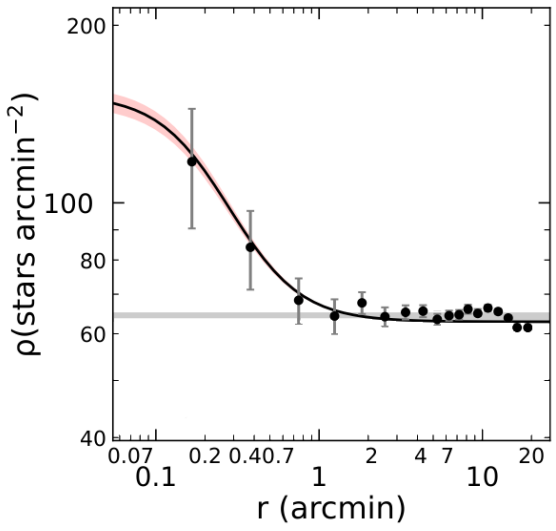

Figure 3. Displayed is the radial density profile of NGC 6793. The black curve corresponds to the RDP profile described by King (1962), with the horizontal grey band marking the stellar density of the background. The red-shaded region highlights the 1σ uncertainty in the King profile fit.

Bukowiecki et al. (2011), which is as follows:

$$r_{\rm lim} = r_{\rm c}\sqrt{\frac{f_0}{3\sigma_{\rm bg}} - 1} \quad (2)$$

Using the formula, we determined the theoretical limiting radius to be 9.93 arcmin. This value aligns closely with the observed limiting radius $r_{\rm lim}^{\rm obs}$, indicating a strong consistency between the theoretical and measured parameters.

3.2. Membership Probabilities of Stars

To distinguish open cluster stars from surrounding field stars, it is essential to account for contamination from both foreground and background stars, especially since open clusters are often located in the Galactic plane. This contamination can hinder the accurate determination of astrophysical parameters, but it can be overcome by utilising proper-motion data, which reflect the common movement of cluster stars formed under similar conditions. The high precision of *Gaia* DR3 data offers a valuable means of distinguishing these stars, as their vector motions are correlated. This makes proper-motion components a crucial factor in membership determination, ensuring that only the cluster stars are included in further analyses, as demonstrated in studies such as those by Bisht et al. (2020). The accuracy of the *Gaia* DR3 data guarantees robust results in these membership studies, facilitating reliable astrophysical assessments.

To calculate the membership probabilities (P) of stars in NGC 6793, we employed the UPMASK method, utilising the precise astrometric data from the *Gaia* DR3 catalogue. This method is based on the k-means clustering technique, which identifies groups of stars with similar proper motions and parallaxes, providing a statistical probability for each star's membership in the cluster. Previous studies have applied this approach successfully (i.e. Cantat-Gaudin et al. 2020; Yontan et al. 2022; Yontan 2023). We performed 100 iterations of the method, using the astrometric parameters (α, δ, $\mu_\alpha \cos\delta$, μ_δ, ϖ) and their uncertainties. A total of 147 stars were identified as members, satisfying the criteria of $P \geq 0.5$, location within the limiting radius, and completeness limit.

To identify the most probable stars of NGC 6793, we generated a vector-point diagram (VPD) by plotting their proper-motion components of the member stars. The VPD, shown in Figure 4, clearly differentiates the NGC 6793 from the surrounding field stars. The blue dashed lines in the diagram represent the mean proper-motion components calculated from $P \geq 0.5$. This visualisation technique is commonly used in studies to isolate cluster members by their kinematic properties, offering a clear separation between cluster stars and foreground or background contamination.

The mean proper-motion components of NGC 6793 were obtained to be ($\mu_\alpha \cos\delta$, μ_δ) = (3.814±0.031, 3.547±0.034) mas yr^{-1}, reflecting the motion of the cluster's member stars. These measurements were derived from the most probable cluster members, which were selected based on their membership probabilities ($P \geq 0.5$). Additionally, we examined the trigonometric parallax data of the identified member stars and plotted the distribution using a histogram. By fitting Gaussian functions to the histogram, we calculated the mean trigonometric parallax value, as shown in Figure 5. The derived trigonometric parallax for NGC 6793 is ϖ=1.674±0.045 mas, providing a direct measure of the cluster's distance from the Sun.

To estimate the distance to NGC 6793, we applied the standard relation d(pc) = 1000/ϖ (mas), which translates the parallax into a distance measurement in parsecs. Using this formula, we found the distance to be d_{ϖ}=597±27 pc. This result is convenient with the findings of other researchers using *Gaia* data, further confirming the accuracy and reliability of our measurement. A detailed comparison with other studies is provided in Table 1, where the values derived for NGC 6793 align well with those reported in the *Gaia* era. This consis-

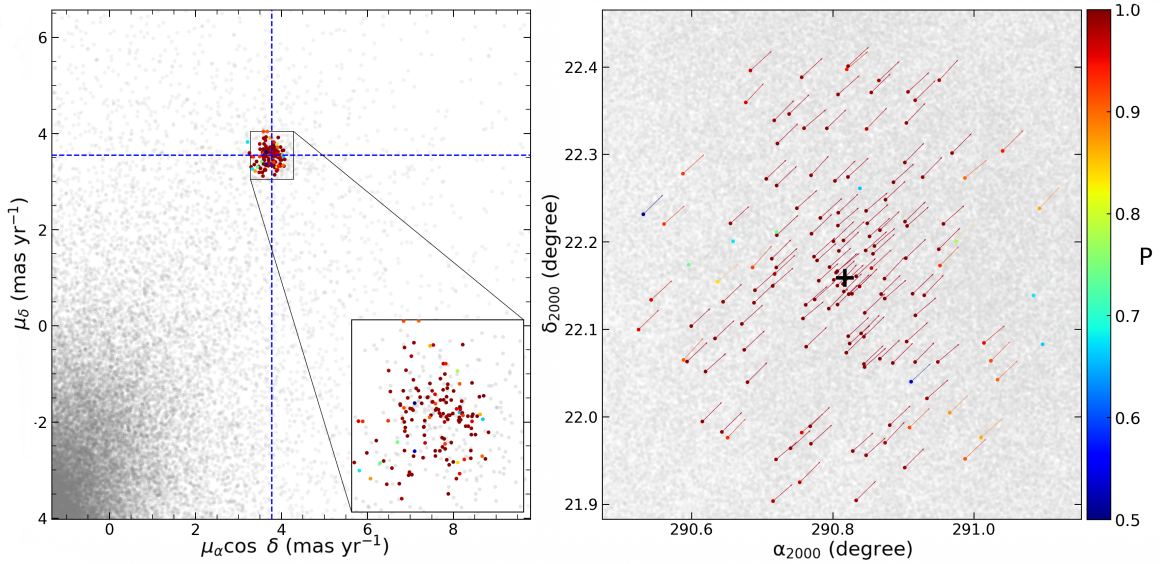

Figure 4. Panel (a) presents the vector-point diagram (VPD), and panel (b) shows the proper-motion velocity vectors for NGC 6793 In the right panel, the colour scale represents most likely member stars ($P \geq 0.5$). In panel (a), the magnified box highlights areas with a high density of member stars in the VPD, while the intersection of blue dashed lines indicates the mean proper motion values. In panel (b), the centre of NGC 6793's equatorial coordinates is marked with black crosshairs.

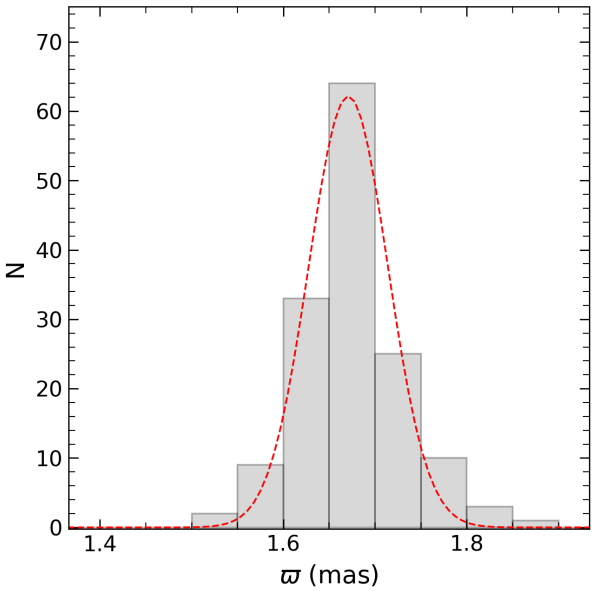

Figure 5. Trigonometric parallax histogram of NGC 6793 from the member stars. The fitted Gaussian function is represented by the red dashed line.

tency underscores the robustness of the *Gaia* astrometric data in determining the fundamental parameters of star clusters.

3.3. Astrophysical Parameters of NGC 6793

In determining fundamental astrophysical parameters, colour-magnitude diagrams (CMDs) serve as crucial instruments. The utilisation of these diagrams facilitates the identification of key features of a cluster, such as the main sequence, turn-off point, and giant stars, which are essential for deriving accurate cluster properties. In this study, we used the CMD derived from the *Gaia* data for the most likely cluster members ($P \geq 0.5$). In order to estimate the age, distance modulus, reddening, and metallicity of NGC 6793, we used the PARSEC stellar isochrones (Bressan et al. 2012). These isochrones, which are specifically designed for the *Gaia* Early Data Release 3 (*Gaia* EDR3; Gaia Collaboration et al. 2021) photometric bands (Riello et al. 2021), were fitted to the observed CMD of the cluster.

To derive the fundamental parameters of NGC 6793, we utilised the $G \times (G_{BP} - G_{RP})$ CMD. Isochrones were fitted through visual comparison, focusing on the most likely members ($P \geq 0.5$) that were identified as part of the main sequence, turn-off point, and giant stars. Before fitting the isochrones, we applied scaling based on the mass fraction z. This procedure provided the *Gaia*-based colour excess of $E(G_{BP} - G_{RP}) = 0.361 \pm 0.035$ mag. To align our results with previous studies, we converted this value to the UBV-based colour excess, $E(B-V)$, using the relation $E(G_{BP} - G_{RP}) = 1.41 \times E(B-V)$ as suggested by Sun et al. (2021). Our resulting value of $E(B-V) = 0.256 \pm 0.025$ mag is consistent with the findings of various studies, confirming agreement across different analyses (see Table 1).

We converted the estimated metallicity [Fe/H] = 0.10 ± 0.05 dex to the mass fraction z in order to select of isochrones as well as for the deriving of fundamental astrophysical parameters. To be able to transform, It is used an analytic expressions of Bovy[2] appropriate for PARSEC isochrones (Bressan et al. 2012; Yontan 2023; Gokmen et al. 2023). The expressions as follow:

$$z_x = 10 \left[[\mathrm{Fe/H}] + \log \left(\frac{z_\odot}{1 - 0.248 - 2.78 \times z_\odot} \right) \right] \quad (3)$$

and

$$z = \frac{(z_x - 0.2485 \times z_x)}{(2.78 \times z_x + 1)}. \quad (4)$$

Here z_x and $z_\odot$ represent intermediate values, with solar metallicity $z_\odot$ adopted as 0.0152 (Bressan et al. 2012). For NGC 6793, we determined a metallicity of $z = 0.0098$.

The PARSEC isochrones with ages of log t (yr) = 8.77, 8.81, and 8.85 and metallicity $z = 0.0098$ were fitted to the observed $G \times (G_{BP} - G_{RP})$ CMD for NGC 6793, as illustrated in Figure 6. The best match was achieved for log t (yr) = 8.81, indicating an age of $t = 650 \pm 50$ Myr for the cluster. This age estimate aligns well with the results reported by Bossini et al. (2019), Zhong et al. (2020), and Cantat-Gaudin et al. (2020) within their quoted uncertainties (see Table 1). The derived distance modulus, $\mu = 9.508 \pm 0.070$ mag, corresponds to an isochrone distance of $d_{iso} = 585 \pm 19$ pc. The uncertainties

[2] https://github.com/jobovy/isodist/blob/master/isodist/Isochrone.py

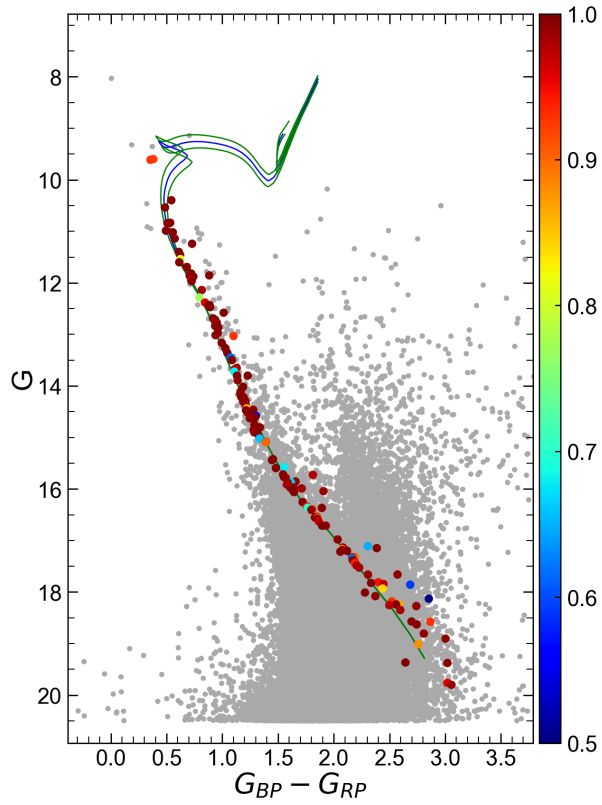

Figure 6. CMD of NGC 6793 is displayed, with different colours representing the member stars of the cluster. The corresponding membership scales are indicated by the colour bars on the right. Stars with probabilities $P < 0.5$ are marked as grey dots. The best-fit PARSEC isochrones are shown in blue, while their uncertainties are illustrated with green lines. The overlaid isochrones correspond to an age of 650 ± 50 Myr for NGC 6793.

in the distance modulus and isochrone distance were estimated using the formulas given by Carraro et al. (2017), which incorporate the uncertainties in photometric magnitudes and excess values of the colour.

The calculated isochrone distance is consistent with the trigonometric parallax distance of $d_{\varpi} = 597 \pm 26$ pc obtained in this study, as well as with the values of Yontan et al. (2019) (see Table 1). Additionally, the Galactocentric coordinates $(X, Y, Z)_{\odot}$ of NGC 6793 were determined. Here, X represents the direction towards the Galactic centre, Y the direction of Galactic rotation, and Z the direction towards the Galactic north pole. Using the isochrone distance along with Galactic coordinates, these coordinates were calculated as $(X, Y, Z)_{\odot} = (325 \pm 18, 485 \pm 22, 34 \pm 6)$ pc. There is strong agreement between these values and those reported by Cantat-Gaudin et al. (2020).

4. LUMINOSITY AND MASS FUNCTIONS

The luminosity function (LF) describes the distribution of stars within the cluster by brightness, while the mass function (MF) characterizes their distribution by stellar masses (Bilir et al. 2006a,b; Canbay et al. 2023).

Since all members of an OC originate simultaneously from the same molecular cloud under comparable physical conditions, these clusters serve as ideal subjects for analyzing stellar distributions in terms of magnitudes and masses. The LF for these cluster members is depicted in Figure 7, and the corresponding mean absolute magnitudes ($\overline{M}_{\rm G}$) are provided in Table 3. The LF exhibits a modest upward trend, indicating that the cluster retains its low to intermediate-mass stars—a characteristic that is rather uncommon for older open clusters in the Milky Way. Based on calculations from the earlier section, the NGC 6793 OC resides in the inner Galactic disc at a Galactocentric distance of 7.69 ± 0.01 kpc, where it experiences significant tidal forces from this region. A connection exists between LF, MF, and the mass-luminosity relation (MLR). For this study, the relation between absolute magnitudes $M_{\rm G}$ and stellar masses $M/M_{\odot}$ provided by Evans et al. (2018) was utilized. This was done for a metallicity of $z = 0.0098$ and $\log t$ (yr) $= 8.81$, covering absolute magnitudes within the range $0.08 < M_{\rm G}$ (mag) ≤ 10.3.

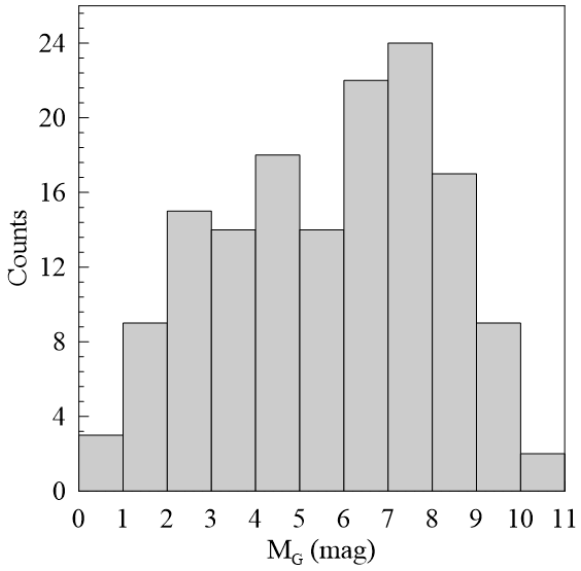

Figure 7. Histograms displaying the distribution of stars along the main sequence within each absolute $M_{\rm G}$ magnitude bin for NGC 6793.

Table 3. Numerical values for the LF, MF, and the fitting parameters, including the slope of the MF for NGC 6793.

Parameter	Value	References
$\overline{M}_{\rm G}$ (mag)	5.66 ± 1.09	This study
$M_{\rm C}$ ($M_{\odot}$)	139 ± 12	This study
$M_{\rm C}$ ($M_{\odot}$)	625.45 ± 74.95	Hunt & Reffert (2024)
$\overline{M}_{\rm C}$ ($M_{\odot}$)	0.949	This study
Γ	1.40 ± 0.26	This study

Once this relationship is established, the total mass of stars and star clusters within a specified magnitude range can be determined by substituting the observed $M_{\rm G}$ values into the corresponding polynomial equation. This approach facilitates the estimation of stellar masses in cases where direct measurements are not feasible, leveraging the accurately calibrated MLR derived from isochrone models. The resulting values are summarized in Table 3.

The mass spectra of open clusters span a wide range of stellar masses, encompassing both very low and high-mass stars. This diversity makes open clusters valuable for investigating the initial mass function (IMF), which represents the primary distribution of stellar masses. The IMF has been extensively explored in previous studies (Phelps & Janes 1993; Piskunov et al. 2004; Yontan 2023; Gokmen et al. 2023; Haroon et al. 2025).

Salpeter (1955) introduced the IMF as a measure of the number of stars (dN) distributed across a logarithmic mass scale (dM) for a given mass M. It is mathematically defined as $dN/dM = M^{-\alpha}$, where $\alpha = (1 + \Gamma)$. The value of α is 2.35, and the present-day mass function (MF) can be expressed as:

$$\log\left(\frac{dN}{dM}\right) = -(1+\Gamma) \times \log(M) + \text{constant} \qquad (5)$$

Here, α is a dimensionless parameter representing the slope

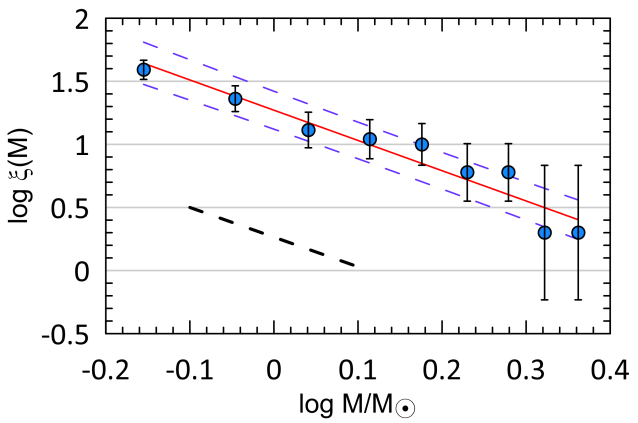

Figure 8. The cluster member mass function, fitted by the power-law of Salpeter (1955) (dashed black line), used to determine the slope (α) for the clusters under investigation.

of the MF, which is illustrated as a straight line in Figure 8. This slope, especially for massive stars ($M > 1\ M_\odot$), acts as a marker for dynamical evolution. Salpeter's power law indicates a rapid decline in the number of stars as mass increases.

In the study, the mass range considered for MF calculations is $0.08 < M_G\ (\mathrm{mag}) \leq 10.3$, encompassing a representative sample of stars. By utilising a least-squares fitting to the MF data, we derived a slope of $\Gamma = 1.40 \pm 0.26$, consistent with Salpeter's value within the margin of uncertainty. Furthermore, the total mass of the cluster (M_C) and the mean stellar mass ($\overline{M/M_\odot}$) for NGC 6793 were calculated as $139 \pm 12\ M_\odot$ and $0.949\ M_\odot$, respectively. These findings are summarized in Table 3.

5. DYNAMICAL RELAXATION AND EVOLUTION TIMES

From a dynamical perspective, the interactions among stars in OCs lead to energy redistribution, distinguishing them from their compact halo counterparts such as globular clusters (Inagaki & Saslaw 1985; Baumgardt & Makino 2003). OCs exhibit a lower spatial density, and processes such as contraction and disruption result in mass segregation, whereby massive stars concentrate closer to the cluster core than their less massive counterparts.This phenomenon has been observed in numerous OCs (Dib & Basu 2018; Bisht et al. 2020).

With respect to kinetic energy, the velocity distribution of stars in OCs tends toward Maxwellian equilibrium (Yadav et al. 2013; Bisht et al. 2019). The time required for this dynamical adjustment is termed the dynamical relaxation time (T_{relax}), during which low-mass stars, possessing greater random velocities, occupy a larger spatial volume compared to massive stars (Mathieu & Latham 1986). The mathematical representation of T_{relax}, which depends on the number of cluster members (N) and the cluster diameter ($D \approx 2r_{\mathrm{lim}}$), is given as follows (Spitzer & Hart 1971; Lada & Lada 2003; Maciejewski & Niedzielski 2007):

$$T_{\mathrm{relax}} = \frac{8.9 \times 10^5 \times N^{1/2} \times R_h^{3/2}}{\overline{M}_C^{1/2} \times \log(0.4 \times N)}, \tag{6}$$

where $\overline{M}_C$ represents the mean stellar mass (in $M_\odot$) and R_h (in pc) is the radius enclosing approximately 50% of the cluster mass. The latter can be derived using the relation (Šablevičiūtė et al. 2006):

$$R_h = 0.547 \times r_c \times \left(\frac{r_t}{r_c}\right)^{0.486}, \tag{7}$$

with r_c and r_t denoting the core and tidal radii, respectively.

Alternatively, T_{relax} can be estimated using the dynamical crossing time ($T_{\mathrm{cross}} = D/\sigma_v$), where $\sigma_v = \sqrt{\sigma_1^2 + \sigma_2^2 + \sigma_3^2}$ is the velocity dispersion (Lada & Lada 2003). The crossing time T_{cross}, defined as the time required for a cluster to complete one passage through the Galaxy, is approximately 10^6 years and is independent of the cluster's size or orbital shape (Binney & Merrifield 1998).

In the Galactic disc, the gravitational influence on massive bodies like star clusters can be expressed using the formula from Röser & Schilbach (2019):

$$x_L = \left(\frac{GM_C}{4A(A-B)}\right)^{1/3} = \left(\frac{GM_C}{4\Omega_o^2 - \kappa^2}\right)^{1/3}, \tag{8}$$

where x_L approximates the cluster's tidal radius (r_t), and $G = 4.30 \times 10^{-6}$ kpc $M_\odot^{-1}$ (km s^{-1})^2 is the gravitational constant. The parameters $\Omega_o = A - B$ and $\kappa = \sqrt{-4B(A-B)}$ represent the angular velocity and the epicyclic frequency at the Sun's position, respectively, with Oort's constants A and B being 15.3 ± 0.4 km s^{-1} kpc^{-1} and -11.9 ± 0.4 km s^{-1} kpc^{-1} (Bovy 2015) or 9.38 ± 0.33 km s^{-1} kpc^{-1} and -16.69 ± 0.25 km s^{-1} kpc^{-1} (Elsanhoury et al. 2025).

Based on our analysis, we estimate $r_t \approx 7.11 \pm 0.38$ pc for NGC 6793. Consequently, the half-mass radius (R_h) is determined to be 0.773 ± 0.01 pc, while the dynamical relaxation time (T_{relax}) is found to be approximately 4.26 Myr.

The dynamical state of the cluster can be characterized by calculating its dynamical evolution parameter, expressed as $\tau = \mathrm{age}/T_{\mathrm{relax}}$. For NGC 6793 OC, τ is found to be significantly greater than 1 ($\tau \gg 1$), indicating that the cluster has reached a state of dynamical relaxation. Subsequently, our attention shifts to estimating the evaporation time ($\tau_{ev} \simeq 10^2 T_{\mathrm{relax}}$), which represents the duration required for internal stellar interactions to completely remove all member stars (Adams & Myers 2001). Low-mass stars continue to escape from the system, primarily at low velocities, exiting through the Lagrange points (Küpper et al. 2008). To maintain the cluster's gravitational binding, the escape velocity (V_{esc}) in the context of rapid gas expulsion is defined as $V_{esc} = R_{gc}\sqrt{2GM_C/3r_t^3}$ (Fich & Tremaine 1991; Fukushige & Heggie 2000). A detailed summary of the derived dynamical parameters, including the corresponding timescales and escape velocity, is provided in Table 4.

Table 4. Dynamical evolution parameters for NGC 6793, including various times and the calculated escape velocity.

Parameter	Value
T_{relax} (Myr)	4.26
τ_{ev} (Myr)	426
τ	153
σ_1 (km s^{-1})	25.43 ± 5.04
σ_2 (km s^{-1})	0.57 ± 0.01
σ_3 (km s^{-1})	0.51 ± 0.01
σ_o (km s^{-1})	25.44 ± 5.04
T_{cross} (Myr)	0.136
V_{esc} (km s^{-1})	222 ± 14.91

6. THE CONVERGENT POINT

To examine the gravitational binding of stellar groups confined within specific regions of the Galactic system, where their motions exhibit parallelism and uniformity, we assessed the velocity ellipsoid parameters (VEPs) and kinematics using computational methods outlined by Bisht et al. (2020) and Elsanhoury et al. (2018). The space velocity vectors (V_x, V_y, V_z) for cluster members are calculated based on their coordinates

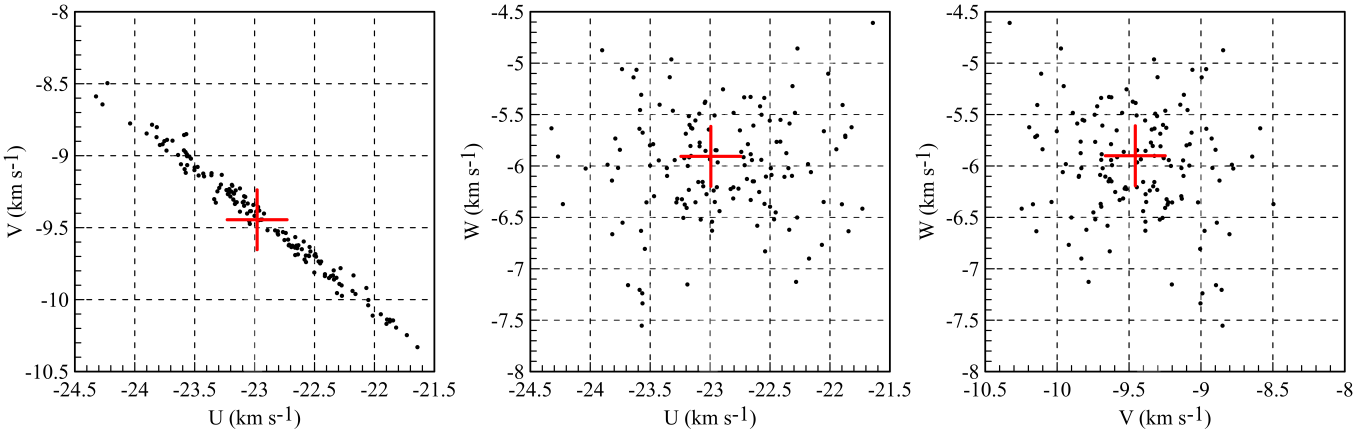

Figure 9. Distribution of the components of space velocity for NGC 6793.

(α, δ), distance (d), proper motion components $(\mu_\alpha \cos\delta, \mu_\delta)$, and mean radial velocity (V_R), using the methodology outlined by Melchior (1958):

$$\begin{pmatrix} V_x \\ V_y \\ V_z \end{pmatrix} = \begin{pmatrix} -4.74\, d\, \mu_\alpha \cos\delta \sin\alpha - 4.74\, d\, \mu_\delta \sin\delta \cos\alpha + V_R \cos\delta \cos\alpha \\ +4.74\, d\, \mu_\alpha \cos\delta \sin\alpha - 4.74\, d\, \mu_\delta \sin\delta \cos\alpha + V_R \cos\delta \cos\alpha \\ +4.74\, d\, \mu_\delta \cos\delta + V_R \sin\delta \end{pmatrix} \quad (9)$$

Our calculations yielded a mean radial velocity for NGC 6793 as $V_R = -20.87 \pm 0.67$ km s^{-1}. Figure 9 illustrates the spatial velocity distribution of the stars most likely associated with NGC 6793. Utilising the computed space velocity components from Equation (9), we derived the Galactic velocity components (U, V, W) using the equatorial-to-Galactic transformation matrix obtained from the SPECFIND v2.0 radio continuum spectra catalogue (Liu et al. 2011), expressed as:

$$\begin{pmatrix} U \\ V \\ W \end{pmatrix} = \begin{pmatrix} -0.05188074\, V_x - 0.87222264\, V_y - 0.48634972\, V_z \\ +0.48469224\, V_x - 0.44779209\, V_y + 0.75136921\, V_z \\ -0.87314490\, V_x - 0.19674834\, V_y + 0.44599133\, V_z \end{pmatrix} \quad (10)$$

Using the solar motion space velocity components provided by Coşkunoğlu et al. (2011), $(U, V, W)_\odot = (8.83 \pm 0.24, 14.19 \pm 0.34, 6.57 \pm 0.21)$ km s^{-1}, we adjusted the space velocity values (U, V, W) of NGC 6793 to the Local Standard of Rest (LSR). The corrected values were found to be $(U, V, W)_{LSR} = (-14.11 \pm 0.25, 4.75 \pm 0.97, 0.67 \pm 0.26)$ km s^{-1}. Based on these corrected components, the total space velocity was calculated as $S_{LSR} = 14.90 \pm 1.04$ km s^{-1}. This velocity aligns well with the range expected for stars belonging to the young thin-disc population (Leggett 1992).

The apex coordinates (A_o, D_o) represent the convergent point toward which the stellar motions within the cluster are directed. This location corresponds to the intersection of the spatial velocity vectors of cluster members with the celestial sphere. Chupina et al. (2001, 2006) proposed a method for calculating apex components in equatorial coordinates, using the mean space velocity vectors derived from Equation (9). These apex coordinates can be determined using the following approach (Elsanhoury 2025):

$$A_o = \tan^{-1}\left(\frac{\overline{V_y}}{\overline{V_x}}\right), \quad D_o = \tan^{-1}\left(\frac{\overline{V_z}}{\sqrt{\overline{V_x^2} + \overline{V_y^2}}}\right) \quad (11)$$

The cross mark in Figure 10 illustrates the apex position for NGC 6793 and their coordinates in Table 5.

Table 5. Calculated dynamical evolution and kinematic parameters for NGC 6793.

Parameter	Value
$\overline{V}_X$ (km s^{-1})	1.82 ± 0.01
$\overline{V}_Y$ (km s^{-1})	25.43 ± 5.04
$\overline{V}_Z$ (km s^{-1})	1.42 ± 0.01
A_o (deg)	85.85 ± 0.11
D_o (deg)	3.12 ± 0 .57
$\overline{U}$ (km s^{-1})	-22.94 ± 0.08
$\overline{V}$ (km s^{-1})	-9.44 ± 0.91
$\overline{W}$ (km s^{-1})	-5.90 ± 0.14

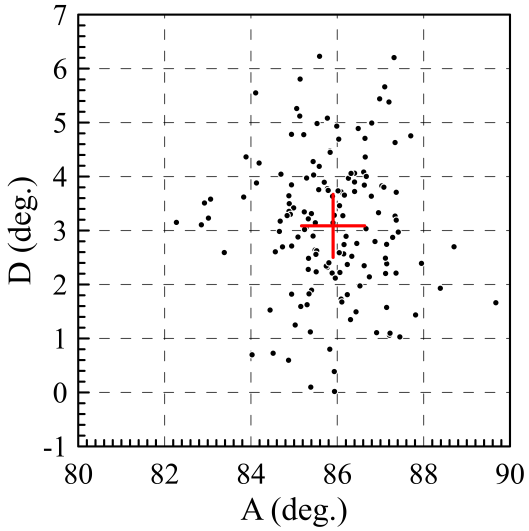

Figure 10. The AD-diagrams for NGC 6793, with a cross mark indicating the position of the apex point $(A_o,\ D_o)$.

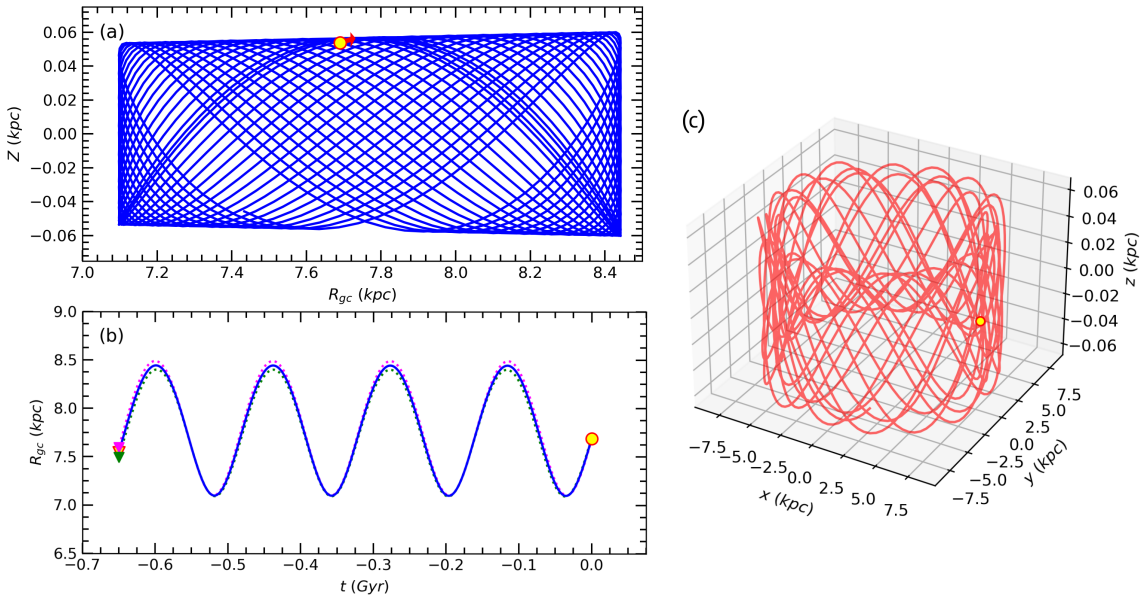

Figure 11. The Galactic trajectories and inferred birth radii of NGC 6793 are presented across three planes: $Z \times R_{gc}$ (a), $R_{gc} \times t$ (b), and X-Y-$Z \times t$ (c). Filled yellow circles mark the OC's current position, while triangles represent the estimated birth locations. The red arrow illustrates the direction of motion. Purple and pink dotted lines trace orbital paths considering uncertainties in the input parameters, with corresponding filled triangles denoting the lower and upper bounds of the birth position estimates.

7. GALACTIC ORBITAL PARAMETERS

The examination of kinematics and orbital dynamics provides crucial insights into the birth locations and Galactic distribution of open clusters (Yontan 2023; Elsanhoury et al. 2025; Taşdemir & Çınar 2025; Yousef Alzahrani et al. 2025b,a). For this study, we analyzed the orbit of NGC 6793 by integrating its motion within the Galactic potential. The analysis used the Python-based GALPY package (Bovy 2015)[3], utilising the MWPOTENTIAL2014 model. This model combines three components: a spherical bulge (Bovy 2015), a disc described by Miyamoto & Nagai (1975), and a spherical dark matter halo based on Navarro et al. (1996). For the calculations, the Galactocentric distance of the Sun was assumed to be $R_{gc} = 8$ kpc, with a rotational velocity of $V_{rot} = 220$ km s^{-1} (Bovy & Tremaine 2012; Bovy 2015).

The Sun's distance from the Galactic plane was adopted as 25 ± 5 pc (Jurić et al. 2008). Radial velocity measurements are essential for orbit integration, and we used *Gaia* DR3 radial velocity data to calculate the mean radial velocity and its uncertainty for NGC 6793. Stars with high membership probabilities ($P \geq 0.5$) were considered, resulting in 58 probable members. A weighted mean approach was applied (see equations in Soubiran et al. 2018), resulting in a mean radial velocity of $V_R = -20.87 \pm 0.67$ km s^{-1}. Comparisons with literature values (Table 1) include -16.59 ± 1.45 km s^{-1} (Soubiran et al. 2018), -25.68 ± 4.71 km s^{-1} (Dias et al. 2021), -37 ± 5.35km s^{-1} (Tarricq et al. 2022) and -20.02 ± 0.76 km s^{-1} (Hunt & Reffert 2024) are in a good agreement. Parameters used for orbit integration include equatorial coordinates ($\alpha = 19^h23^m16^s.08$, $\delta = +22°09'32''.3$) from Cantat-Gaudin et al. (2020), proper motions ($\mu_\alpha \cos\delta$, μ_δ = 3.814±0.031, 3.547±0.034 mas yr^{-1}) derived in Section 3.2, an isochrone distance ($d_{iso} = 585 \pm 19$ pc) from Section 3.3 and presented in Table 6.

The orbit of NGC 6793 was integrated forward with a time step of 1 Myr over 2.5 Gyr to determine its likely current position. Figure 11a depicts the cluster's path on the $Z \times R_{gc}$ plane, showing its height above the Galactic plane and distance from the Galactic centre. To trace the cluster's origin, backward integration was performed for a duration matching its estimated age (650 Myr). The integration period did not exceed the cluster's age, to minimise potential inaccuracies due to model limitations and observational uncertainties, including errors in distance, proper motion, and radial velocity (Gaia Collaboration et al. 2018; Sariya et al. 2021). Figure 11b illustrates the time evolution of the cluster's Galactocentric distance on the $R_{gc} \times t$ plane, accounting for input parameter variations. The results indicate an uncertainty of approximately 0.09 pc for the cluster's birth radius, suggesting that NGC 6793 formed outside the solar neighborhood,, with an estimated birth radius of 7.54 kpc.

Orbit integration for NGC 6793 yielded the following orbital parameters: apogalactic ($R_a = 8442 \pm 43$ pc) and perigalactic ($R_p = 7098 \pm 5$ pc) distances, eccentricity ($e = 0.087 \pm 0.003$), maximum vertical distance from the Galactic plane ($Z_{max} = 60 \pm 1$ pc) and orbital period ($P_{orb} = 217 \pm 1$ Myr). The calculated apogalactic and perigalactic distances indicate that the orbit of NGC 6793 lies entirely beyond the solar circle (Figure 11a). The maximum height above the Galactic plane, $Z_{max} = 60 \pm 1$ pc, further suggests that NGC 6793 is a member of the thin-disc population of the Milky Way (Bilir et al. 2006a,c, 2008; Evcil et al. 2024; Canbay et al. 2025; Çınar et al. 2025).

[3] https://galpy.readthedocs.io/en/v1.5.0/

8. SUMMARY AND CONCLUSION

In this study, we conducted a comprehensive analysis of the open cluster NGC 6793, utilizing *Gaia* DR3 data for photometric, astrometric, and kinematic assessments. A total of 147 stars were identified as the most probable members based on membership probabilities $P \geq 0.5$. These member stars served as the foundation for deriving key astrophysical and Galactic orbital parameters. The cluster's age, distance modulus, and reddening were simultaneously determined from the *Gaia*-based CMD. A summary of the key findings is presented in Table 6. The results from this study can be outlined as follows:

Table 6. Fundamental parameters of NGC 6793.

Parameter	Value
$(\alpha,\ \delta)_{\rm J2000}$	$19^{\rm h}23^{\rm m}16^{\rm s}.08$, $+22^{\rm o}09'32''.3$
$(l, b)_{\rm J2000}$	56.18600, +3.31804
f_0 (stars arcmin^{-2})	89.628±5.878
$f_{\rm bg}$ (stars arcmin^{-2})	62.855±0.750
$r_{\rm c}$ (arcmin)	1.593±0.128
$r_{\rm c}$ (pc)	0.28±0.01
$r_{\rm lim}$ (arcmin)	10
$r_{\rm lim}$ (pc)	1.70
$r_{\rm t}$ (pc)	7.11±0.38
$R_{\rm h}$ (pc)	0.773±0.01
Cluster members ($P \geq 0.5$)	147
$\mu_\alpha \cos\delta$ (mas yr^{-1})	3.814 ± 0.031
μ_δ (mas yr^{-1})	3.547 ± 0.034
ϖ (mas)	1.674 ± 0.045
d_ϖ (pc)	597 ± 26
$E(B-V)$ (mag)	0.256 ± 0.025
$E(G_{\rm BP}-G_{\rm RP})$ (mag)	0.361 ± 0.035
$A_{\rm G}$ (mag)	0.672 ± 0.065
[Fe/H] (dex)	0.10 ± 0.05
Age (Myr)	650 ± 50
Distance modulus (mag)	9.508 ± 0.070
Isochrone distance (pc)	585 ± 19
$(X, Y, Z)_\odot$ (pc)	(325 ± 18, 485 ± 22, 34 ± 6)
$R_{\rm gc}$ (kpc)	7.69 ± 0.01
MF slope	1.40 ± 0.26
Total mass ($M_\odot$)	139 ± 12
$V_{\rm R}$ (km s^{-1})	-20.87 ± 0.67
$U_{\rm LSR}$ (km s^{-1})	−14.11 ± 0.25
$V_{\rm LSR}$ (kms^{-1})	4.75 ± 0.97
$W_{\rm LSR}$ (kms^{-1})	0.67 ± 0.26
$S_{\rm LSR}$ (kms^{-1})	14.90 ± 1.04
$R_{\rm a}$ (pc)	8442 ± 43
$R_{\rm p}$ (pc)	7098 ± 5
$z_{\rm max}$ (pc)	60 ± 1
e	0.087 ± 0.003
$P_{\rm orb}$ (Myr)	217 ± 1
Birthplace (pc)	7542 ± 99

1. We performed a detailed analysis of the radial distribution of stars in NGC 6793 to derive its structural parameters. The background stellar density, central density, and core radius were estimated to be $f_{\rm bg} = 62.855 \pm 0.750$ stars arcmin^{-2}, $f_0 = 89.628 \pm 5.878$ stars arcmin^{-2}, and $r_{\rm c} = 1.593 \pm 0.128$ arcmin, respectively. The outermost boundary of the cluster was defined by the point where the radial density profile (RDP) aligns with the background stellar density. Based on this fitting, the limiting radius of the cluster was determined to be $r_{\rm lim}^{\rm obs} = 10$ arcmin.

2. Using the vector point diagram (VPD), we calculated the mean proper motion components for NGC 6793, obtaining as $(\mu_\alpha \cos\delta,\ \mu_\delta) = (3.814 \pm 0.031,\ 3.547 \pm 0.034)$ mas yr^{-1}.

3. The colour excess for NGC 6793, derived from *Gaia* data, was determined as $E(G_{\rm BP} - G_{\rm RP}) = 0.361 \pm 0.035$ mag by comparing the cluster's CMD with theoretical isochrones from Bressan et al. (2012) at $z = 0.0098$. Using the relation $E(G_{\rm BP} - G_{\rm RP}) = 1.41 \times E(B-V)$ from Sun et al. (2021), we estimated the *UBV*-system colour excess as $E(B-V) = 0.256 \pm 0.025$ mag.

4. The distance to NGC 6793, derived from isochrone fitting, was found to be $d_{\rm iso} = 585 \pm 19$ pc, which closely corresponds to the distance calculated from the trigonometric parallax, $d_\varpi = 597 \pm 26$ pc. The age of the cluster was estimated to be $t = 650 \pm 50$ Myr, based on the comparison between the observed CMD and the isochrone model from Bressan et al. (2012) with $z = 0.0098$.

5. The mass function slope of NGC 6793 was determined to be $\Gamma = 1.40 \pm 0.26$, which is in close agreement with the classic Salpeter value of 2.35 (Salpeter 1955). The total cluster mass was estimated as approximately $139 \pm 12\ M/M_\odot$. Yontan et al. (2019) derived a mass function slope for NFC 6793 of $\Gamma = 1.31 \pm 0.31$ which is in good agreement with our findings.

6. The analysis of the evolutionary timescales of NGC 6793 reveals that the cluster is dynamically relaxed, as the dynamical evolution parameter $\tau \gg 1$.

7. Equatorial coordinates of the coherent convergent point were computed using the well-known AD-diagram method, and found to be $(A_{\rm o},\ D_{\rm o}) = (85^{\rm o}.85 \pm 0^{\rm o}.11,\ 3^{\rm o}.12 \pm 0^{\rm o}.57)$.

8. Galactic orbit analysis revealed that NGC 6793 follows an elliptical orbit outside the solar radius, situated within the young thin-disc population of the Milky Way. Additionally, the estimated birth radius of the cluster, $\sim 7.54 \pm 0.01$ kpc, suggests that it originated beyond the solar neighbourhood.

Peer Review: Externally peer-reviewed.

Author Contribution: Conception/Design of study - S.T., D.C.Ç., S.T.; Data Acquisition - S.T., D.C.Ç.; Data Analysis/Interpretation - S.T., D.C.Ç., R.C., W.H.E., A.A.H.; Drafting Manuscript - S.T., D.C.Ç.; Critical Revision of Manuscript - S.T., D.C.Ç.; Final Approval and Accountability - S.T., D.C.Ç.

Conflict of Interest: Authors declared no conflict of interest.

Financial Disclosure: This study has been supported in part by the Scientific and Technological Research Council (TÜBİTAK) 122F109.

Acknowledgements: This research has made use of the WEBDA database, operated at the Department of Theoretical Physics and Astrophysics of the Masaryk University. We also made use of NASA's Astrophysics Data System as well as the VizieR and Simbad databases at CDS, Strasbourg, France and data from the European Space Agency (ESA) mission *Gaia*[4], processed by the *Gaia* Data Processing and Analysis Consortium (DPAC)[5]. Funding for DPAC has been provided by national institutions, in particular, the institutions participating in the *Gaia* Multilateral Agreement.

LIST OF AUTHOR ORCIDS

S. Taşdemir https://orcid.org/0000-0003-1339-9148
D. C. Çınar https://orcid.org/0000-0001-7940-3731
R. Canbay https://orcid.org/0000-0003-2575-9892
S. Taştan https://orcid.org/0009-0009-3372-3663
W. H. Elsanhoury https://orcid.org/0000-0002-2298-4026
Haroon A. A. https://orcid.org/0000-0002-8194-5836

REFERENCES

Adams F. C., Myers P. C., 2001, ApJ, 553, 744
Bastian N., Covey K. R., Meyer M. R., 2010, ARA&A, 48, 339
Baumgardt H., Makino J., 2003, MNRAS, 340, 227
Bilir S., Karaali S., Ak S., Yaz E., Hamzaoğlu E., 2006a, New Astron., 12, 234
Bilir S., Güver T., Aslan M., 2006b, Astronomische Nachrichten, 327, 693
Bilir S., Karaali S., Gilmore G., 2006c, MNRAS, 366, 1295
Bilir S., Cabrera-Lavers A., Karaali S., Ak S., Yaz E., López-Corredoira M., 2008, Publ. Astron. Soc. Australia, 25, 69
Binney J., Merrifield M., 1998, Galactic Astronomy
Binney J., Tremaine S., 2008, Galactic Dynamics, 2nd edn. Princeton University Press
Bisht D., Yadav R. K. S., Ganesh S., Durgapal A. K., Rangwal G., Fynbo J. P. U., 2019, MNRAS, 482, 1471
Bisht D., Zhu Q., Yadav R. K. S., Durgapal A., Rangwal G., 2020, MNRAS, 494, 607
Bossini D., et al., 2019, A&A, 623, A108
Bovy J., 2015, ApJS, 216, 29
Bovy J., Tremaine S., 2012, ApJ, 756, 89
Bressan A., Marigo P., Girardi L., Salasnich B., Dal Cero C., Rubele S., Nanni A., 2012, MNRAS, 427, 127
Bukowiecki Ł., Maciejewski G., Konorski P., Strobel A., 2011, Acta Astron., 61, 231
Canbay R., Bilir S., Özdönmez A., Ak T., 2023, AJ, 165, 163
Canbay R., AK T., Bilir S., Soydugan F., Eker Z., 2025, AJ, 169, 87
Cantat-Gaudin T., Anders F., 2020, A&A, 633, A99
Cantat-Gaudin T., et al., 2020, A&A, 640, A1
Carraro G., Sales Silva J. V., Moni Bidin C., Vazquez R. A., 2017, AJ, 153, 99
Chupina N. V., Reva V. G., Vereshchagin S. V., 2001, A&A, 371, 115
Chupina N. V., Reva V. G., Vereshchagin S. V., 2006, A&A, 451, 909
Coşkunoğlu B., et al., 2011, MNRAS, 412, 1237
Dias W. S., Monteir H., Moitinho A., Lépine J. R. D., Carraro G., Paunzen E., Alessi B., Villela L., 2021, MNRAS, 504, 356
Dib S., Basu S., 2018, A&A, 614, A43
Donada J., et al., 2023, A&A, 675, A89
Elsanhoury W. H., 2025, Astronomische Nachrichten, 346, e20240082
Elsanhoury W. H., Postnikova E. S., Chupina N. V., Vereshchagin S. V., Sariya D. P., Yadav R. K. S., Jiang I.-G., 2018, Ap&SS, 363, 58
Elsanhoury W. H., Haroon A. A., Elkholy E. A., Çınar D. C., 2025, Journal of Astrophysics and Astronomy, 46, 21
Evans D. W., et al., 2018, A&A, 616, A4
Evcil S., Adalalı S., Alan N., Canbay R., Bilir S., 2024, Astronomische Nachrichten, 345, e20240038
Fich M., Tremaine S., 1991, ARA&A, 29, 409
Fukushige T., Heggie D. C., 2000, MNRAS, 318, 753
Gaia Collaboration et al., 2018, A&A, 616, A1
Gaia Collaboration et al., 2021, A&A, 649, A1
Gaia Collaboration et al., 2023, A&A, 674, A1
Gokmen S., Eker Z., Yontan T., Bilir S., Ak T., Ak S., Banks T., Sarajedini A., 2023, AJ, 166, 263
Haroon A. A., Elsanhoury W. H., Elkholy E. A., Saad A. S., Çınar D. C., 2025, Phys. Scr., 100, 055006
Hunt E. L., Reffert S., 2024, A&A, 686, A42
Inagaki S., Saslaw W. C., 1985, ApJ, 292, 339
Joshi Y. C., Dambis A. K., Pandey A. K., Joshi S., 2016, A&A, 593, A116
Jurić M., et al., 2008, ApJ, 673, 864
King I., 1962, AJ, 67, 471
Kroupa P., 2001, MNRAS, 322, 231
Küpper A. H. W., MacLeod A., Heggie D. C., 2008, MNRAS, 387, 1248
Lada C. J., Lada E. A., 2003, ARA&A, 41, 57
Leggett S. K., 1992, ApJS, 82, 351
Liu L., Pang X., 2019, ApJS, 245, 32
Liu J. C., Zhu Z., Hu B., 2011, A&A, 536, A102
Maciejewski G., Niedzielski A., 2007, A&A, 467, 1065
Mathieu R. D., Latham D. W., 1986, AJ, 92, 1364
Melchior P. J., 1958, Ciel et Terre, 74, 290
Miyamoto M., Nagai R., 1975, PASJ, 27, 533
Navarro J. F., Frenk C. S., White S. D. M., 1996, ApJ, 462, 563
Perryman M. A. C., et al., 1998, A&A, 331, 81
Phelps R. L., Janes K. A., 1993, AJ, 106, 1870
Piskunov A. E., Belikov A. N., Kharchenko N. V., Sagar R., Subramaniam A., 2004, MNRAS, 349, 1449
Poggio E., et al., 2021, A&A, 651, A104
Riello M., et al., 2021, A&A, 649, A3
Röser S., Schilbach E., 2019, A&A, 627, A4
Salpeter E. E., 1955, ApJ, 121, 161
Sariya D. P., et al., 2021, AJ, 161, 101
Soubiran C., et al., 2018, A&A, 619, A155
Spitzer Jr. L., Hart M. H., 1971, ApJ, 164, 399
Sun M., Jiang B., Yuan H., Li J., 2021, ApJS, 254, 38
Taşdemir S., Çınar D. C., 2025, Contributions of the Astronomical Observatory Skalnaté Pleso, 55, 506
Tarricq Y., et al., 2021, A&A, 647, A19
Tarricq Y., Soubiran C., Casamiquela L., Castro-Ginard A., Olivares J., Miret-Roig N., Galli P. A. B., 2022, A&A, 659, A59
Yadav R. K. S., Sariya D. P., Sagar R., 2013, MNRAS, 430, 3350
Yontan T., 2023, AJ, 165, 79

[4] https://www.cosmos.esa.int/gaia
[5] https://www.cosmos.esa.int/web/gaia/dpac/consortium

Yontan T., et al., 2019, Astrophysics and Space Science, 364, 152

Yontan T., et al., 2022, Rev. Mex. Astron. Astrofis., 58, 333

Yousef Alzahrani A., Haroon A., Elsanhoury W., Çınar D. C., 2025a, arXiv e-prints, p. arXiv:2504.15341

Yousef Alzahrani A., Haroon A., Elsanhoury W., Çınar D. C., 2025b, arXiv e-prints, p. arXiv:2504.15344

Zhong J., Chen L., Wu D., Li L., Bai L., Hou J., 2020, A&A, 640, A127

Çınar D. C., Bilir S., Şahin T., Plevne O., 2025, AJ, 170, 13

Šablevičiūtė I., Vansevičius V., Kodaira K., Narbutis D., Stonkutė R., Bridžius A., 2006, Baltic Astronomy, 15, 547